Computational Mechanics 19 (1997) 397–410 © Springer-Verlag 1997

Optimal design of piezoelectric microstructures

E. C. Nelli Silva, J. S. Ono Fonseca, N. Kikuchi

Abstract Application of piezoelectric materials requires an improvement in their performance characteristics which can be obtained by designing new topologies of microstructures (or unit cells) for these materials. The topology of the unit cell (and the properties of its constituents) determines the effective properties of the piezocomposite. By changing the unit cell topology, better performance characteristics can be obtained in the piezocomposite. Based on this idea, we have proposed in this work an optimal design method of piezocomposite microstructures using topology optimization techniques and homogenization theory. The topology optimization method consists of finding the distribution of material phase and void phase in a periodic unit cell, that optimizes the performance characteristics, subject to constraints such as property symmetry and stiffness. The optimization procedure is implemented using sequential linear programming. In order to calculate the effective properties of a unit cell with complex topology, a general homogenization method applied to piezoelectricity was implemented using the finite element method. This method has no limitations regarding volume fraction or shape of the composite constituents. Although only two-dimensional plane strain topologies of microstructures have been considered to show the implementation of the method, this can be extended to three-dimensional topologies. Microstructures obtained show a large improvement in performance characteristics compared to pure piezoelectric material or simple designs of piezocomposite unit cells.

Communicated by S. N. Atluri, 18 November 1996

E. C. Nelli Silva[1]
Department of Mechanical Engineering of Polytechnic School at the University of São Paulo, São Paulo, Brazil

J. S. Ono Fonseca, N. Kikuchi
Department of Mechanical Engineering and Applied Mechanics, The University of Michigan, Ann Arbor, MI, 48109-2125, USA

[1]*Present address*: Department of Mechanical Engineering and Applied Mechanics, The University of Michigan, Ann Arbor, MI, 48109-2125, USA

Correspondence to: E. C. Nelli Silva

The first two authors thank CNPq-Conselho Nacional de Desenvolvimento Científico e Tecnológico (Brazilian National Council for Scientific and Technologic Development) for supporting them in their graduate studies. The authors are thankful for the financial support received through a Maxwell Project (ONR 00014-94-1-022 and US Army TACOM DAAE 07-93-C-R125).

1 Introduction

Piezoelectric materials have the property of converting electrical energy (electric field and applied electrical charge) into mechanical energy (strain and stress) and vice versa. They are widely used in electromechanical sensors and actuators such as robotics sensors, ultrasonic transducers for medical imaging and non destructive evaluation (NDE), underwater acoustics (some hydrophones and naval sonars), and other applications. The main goal in the transducer design in all these applications is to increase the response of the transducer which can be achieved, for example, by increasing the electromechanical energy conversion. The energy conversion depends on many factors, one of the most important being the properties of the piezoelectric material. In this work, we consider ultrasonic imaging and naval sonar applications. In these applications, it is well known that materials such as "1–3 piezocomposite" (piezoceramic rods embedded in a soft polymer matrix) allow greater sensitivity, in both low and high frequency applications, than pure piezoceramic (see Smith and Auld 1991, and Smith 1993). This improvement occurs because the composite material provides effective properties (elastic, piezoelectric, and dielectric) that produce a better performance than pure piezoelectric materials. These effective (homogenized) properties can be determined by considering the topology of the composite microstructure (or unit cell, the smallest structure that is periodic in the composite) and the properties of its constituents.

In this sense, many previous papers have reported the study of performance maximization by changing the volume fraction of ceramic rods, its properties, its shape (see Hossack and Hayward 1991, and Hayward and Bennett 1996), and the mechanical properties of the polymer matrix in the composite unit cell. Smith (1991), and Avellaneda and Swart (1994) showed that the use of negative Poisson's ratio polymer matrix greatly increases the performance of the composite. Avellaneda and Swart (1994) also determined that the presence of porosity in the polymer matrix enhances the piezocomposite response. In all these studies, the polymer phase (matrix) is considered to be an isotropic material. Departing from the isotropic assumption and considering a transverse isotropic polymer, Gibiansky and Torquato (1995) extended the Avellaneda and Swart (1994) analysis by optimizing the properties of the matrix polymer that enhance the per-

formance characteristics of the piezocomposite. The solution obtained consists of a polymer matrix with given properties that are highly anisotropic, weakened by an optimal arrangement of pores. Although the piezoelectric effect was taken into account, the design of the polymer matrix unit cell was separate from the piezoelectric inclusion. Therefore, in relation to the dimensions of the piezoelectric inclusion, the matrix is uniform in the piezocomposite unit cell. The design of the matrix microstructure topology with specified properties is complex and is obtained using the method described in Sigmund (1995).

In this work, we change the topology of the piezoelectric material in the unit cell in order to determine the optimal design of the piezocomposite microstructure with high performance characteristic. The distribution of the two phases (material phase and void phase) is determined in the composite unit cell by using the topology optimization procedure. A general homogenization method for piezoelectricity was implemented using the finite element method, in order to calculate the effective properties of the piezocomposite. This homogenization has no limitations regarding volume fraction or shape of the composite constituents. Performance characteristics are measured differently depending on the application of the piezoelectric material – low frequency applications such as hydrophones or high frequency applications such as transducers for ultrasonic imaging.

Fonseca and Kikuchi (1995), and Sigmund (1995) initially developed the topology design of microstructures for elastic materials using the homogenization method and topology optimization techniques. With this method, microstructures with specified properties can be obtained. The method is general and the only limitations for the specification of the achievable properties lie in the thermodynamic considerations (which determine that the elastic tensor must be positive definite) and the bounds defined by Hashin and Shtrikman (1963). It is possible to design material microstructures with unusual behavior determined by extremal properties, as in negative Poisson's ratio material (see Fonseca and Kikuchi 1996). The method was extended to the design of thermoelastic microstructures in Sigmund and Torquato (1996).

In the case of piezoelectric material, a new set of properties, in the space of achievable properties, that maximizes the performance characteristics must be found. This can be achieved by designing the unit cell of the piezocomposite material using a similar procedure as in the case of elastic structures. The space of achievable properties for the piezocomposite material is also dictated by thermodynamic considerations that require positive definiteness of the tensor involving the elastic, piezoelectric, and dielectric properties, as discussed in Smith (1992). Other bounds however, are not available for piezoelectric materials in the literature.

Although the method introduced in this work is general and can be applied in the design of 3D microstructures, the examples presented herein are limited to 2D plane strain microstructure due to its lower computational cost. Plane stress condition can also be considered but it is less realistic (due to manufacturing considerations) than plane strain for representing the piezoelectric material operation in a ultrasonic transducer or hydrophone.

This paper is organized as follows: In section 2, the constitutive equations of the piezoelectric medium are presented in their most common forms. In section 3, the quantities that describe the performance characteristics of the transducer for low and high frequency applications are given. In section 4, the theoretical formulation and numerical implementation of the homogenization method applied to piezoelectricity are presented. In section 5, the optimization problem and its parameters are defined. In section 6, some microstructure topologies resulting from the optimization and a discussion of the results are presented. In section 7, some conclusions are given. The symmetry conditions for homogenization are briefly presented in appendix A and the sensitivity analysis of the material properties necessary for the optimization problem are derived in appendix B.

2
Constitutive equations of piezoelectric materials

In this section, a brief description of the constitutive equations of piezoelectric materials is given, and the properties of piezoelectric medium are defined. These properties will be used for expressing the performance characteristics in the next section.

This paper considers piezoelectric materials that respond linearly to changes in the electric field, electric displacement, or mechanical stress and strain. Variations in temperature and magnetic field are considered unimportant. This is compatible with the piezoelectric ceramics, polymers, and composites in current use (see Smith 1992). With these assumptions, the behavior of the piezoelectric medium is described by the following piezoelectric constitutive equations which relate the stress (T_{ij}), strain (S_{kl}), electric field (E_k), and electric displacement (D_i) (see IEEE 1984):

$$\begin{cases} T_{ij} = c^E_{ijkl} S_{kl} - e_{kij} E_k \\ D_i = e_{ikl} S_{kl} + \epsilon^S_{ik} E_k \end{cases} \tag{1}$$

where c^E_{ijkl} is a fourth order stiffness tensor under short circuit boundary conditions, ϵ^S_{ik} is a second order free-body electric tensor, and e_{kij} is a third order piezoelectric strain tensor.

Due to the symmetry of the tensors $T_{ij}, S_{ij}, c^E_{ijkl}$, and ϵ^S_{ij}, Eq. (1) can be written in a compact notation (see IEEE 1984):

$$\begin{cases} T_P = c^E_{PQ} S_Q - e_{Pk} E_k \\ D_i = e_{iQ} S_Q + \epsilon^S_{ik} E_k \end{cases} \text{ or } \begin{cases} \mathbf{T} = \mathbf{c}^E \mathbf{S} - \mathbf{e}\mathbf{E} \\ \mathbf{D} = \mathbf{e}^t \mathbf{S} + \boldsymbol{\epsilon}^S \mathbf{E} \end{cases} \tag{2}$$

where $\mathbf{c}^E = c^E_{PQ}, \boldsymbol{\epsilon}^S = \epsilon^S_{ik}, \mathbf{e} = e_{iQ}, \mathbf{S} = S_{ij} = S_P$ when $i = j$, $p = 1, 2, 3$, and $2S_{ij} = S_P$ when $i \neq j$, $p = 4, 5, 6$. The superscript "t" denotes a transposed matrix. Similar relations hold for the other terms in (2) (see IEEE 1984).

The constitutive equations can also be represented by an alternate form:

$$\begin{cases} \mathbf{S} = \mathbf{s}^E \mathbf{T} + \mathbf{d}\mathbf{E} \\ \mathbf{D} = \mathbf{d}^t \mathbf{T} + \boldsymbol{\epsilon}^T \mathbf{E} \end{cases} \tag{3}$$

where $\mathbf{s}^{\mathrm{E}}$ is the compliance tensor under short circuit conditions, $\boldsymbol{\epsilon}^T$ is the clamped body dielectric tensor, and $\mathbf{d}$ is the piezoelectric stress tensor. The relations among the coefficients are (see IEEE 1984):

$$\mathbf{s}^E = (\mathbf{c}^E)^{-1} \quad \boldsymbol{\epsilon}^T = \boldsymbol{\epsilon}^S + \mathbf{d}^t(\mathbf{s}^E)^{-1}\mathbf{d} \quad \mathbf{d} = (\mathbf{s}^E)\mathbf{e} \tag{4}$$

In the case of a piezocomposite made, for example, of PZT ceramic rods embedded in a polymer, if the wavelength of the applied field is much larger than the spacing between rods, the composite material can be modelled as a homogeneous medium. In this case, its behavior can be characterized by the previous Eqs. (2) and (3) considering the composite effective properties (or homogenized properties) in these equations (see Smith and Auld 1991, and Smith 1993). These effective properties can be obtained using the homogenization method presented in section 4. Therefore, the constitutive equations of the composite material considering homogenized properties become:

$$\begin{cases} \langle \mathbf{T} \rangle = \mathbf{c}_H^E \langle \mathbf{S} \rangle - \mathbf{e}_H \langle \mathbf{E} \rangle \\ \langle \mathbf{D} \rangle = \mathbf{e}_H^t \langle \mathbf{S} \rangle + \boldsymbol{\epsilon}_H^S \langle \mathbf{E} \rangle \end{cases} \tag{5}$$

$$\begin{cases} \langle \mathbf{S} \rangle = \mathbf{s}_H^E \langle \mathbf{T} \rangle - \mathbf{d}_H \langle \mathbf{E} \rangle \\ \langle \mathbf{D} \rangle = \mathbf{d}_H^t \langle \mathbf{T} \rangle + \boldsymbol{\epsilon}_H^T \langle \mathbf{E} \rangle \end{cases} \tag{6}$$

where $\langle . \rangle$ denotes volume averaged quantities and the subscript "H" refers to the homogenized properties. The relations among the properties become:

$$\mathbf{s}_H^E = (\mathbf{c}_H^E)^{-1} \quad \boldsymbol{\epsilon}_H^T = \boldsymbol{\epsilon}_H^S + \mathbf{d}_H^t(\mathbf{s}_H^E)^{-1}\mathbf{d}_H \quad \mathbf{d}_H = (\mathbf{s}_H^E)\mathbf{e}_H \tag{7}$$

In the following sections, the subscript "H" will be omitted for the homogenized properties for the sake of brevity.

3 Piezocomposite materials performance characteristics

In this section, a brief summary of the expressions that describe the performance characteristics of piezocomposites is given. Two kinds of applications are considered: low frequency (hydrostatic operation mode, such as some hydrophones) and high frequency (medical ultrasonic imaging or therapy).

3.1 Low frequency applications

Considering a transversely isotropic composite under hydrostatic pressure $\langle T \rangle = T\delta_{ij}$ (δ_{ij} is the Kronecker delta), the composite's responses are given by three quantities (see Avellaneda and Swart 1994):

- Hydrostatic Coupling Coefficient (d_h)

$$d_h = \langle D_3 \rangle / T = d_{33} + 2d_{13} \tag{8}$$

- Figure of Merit ($d_h \mathrm{g_h}$)

$$d_h \mathrm{g_h} = \mathrm{d_h^2} = \mathrm{d_h^2}/\epsilon_{33}^{\mathrm{T}} \tag{9}$$

- Hydrostatic Electromechanical Coupling Factor (k_h)

$$k_h = \sqrt{\frac{d_h^2}{\epsilon_{33}^T s_h^E}} \tag{10}$$

where $s_h^E = 2s_{11}^E + 2s_{12}^E + 4s_{13}^E + s_{33}^E$ is the dilatational compliance, and the coefficients s_{kl}^E are those defined in Eq. (6). The coefficient k_h measures the overall acoustic/electric power conversion.

In terms of the properties described in Eq. (5), these quantities can be written as given by Avellaneda and Swart (1994), and Gibiansky and Torquato (1995):

$$\begin{aligned} d_h &= \mathbf{v}\mathbf{C}^{-1}\mathbf{e} \quad d_h \mathrm{g_h} = \frac{(\mathbf{v}\mathbf{C}^{-1}\mathbf{e})^2}{\epsilon_{33} + \mathbf{e}^{\mathrm{t}}\mathbf{C}^{-1}\mathbf{e}} \\ k_h^2 &= \frac{(\mathbf{v}\mathbf{C}^{-1}\mathbf{e})^2}{(\epsilon_{33} + \mathbf{e}^t\mathbf{C}^{-1}\mathbf{e})\mathbf{v}\mathbf{C}^{-1}\mathbf{v}^t} \end{aligned} \tag{11}$$

where:

$$\mathbf{C} = \begin{pmatrix} K & c_{13} \\ c_{13} & c_{33} \end{pmatrix} \quad \mathbf{e} = \begin{pmatrix} e_{11} \\ e_{33} \end{pmatrix} \quad \mathbf{v} = \begin{pmatrix} 1 & 1 \end{pmatrix} \tag{12}$$

and $K = (c_{11} + c_{12})/2$ is the transverse bulk modulus. All the properties considered in the definitions are homogenized properties.

However, in this work only 2D plane strain microstructures in the 1–3 (or xz) plane were considered. Therefore, quantities $d_h, d_h \mathrm{g_h}$, and k_h were redefined in Eqs. (11) considering a new matrix $\mathbf{C}$:

$$\mathbf{C} = \begin{pmatrix} c_{11} & c_{13} \\ c_{13} & c_{33} \end{pmatrix} \tag{13}$$

resulting in the expressions for the performance characteristics of the 2D plane strain case. This new matrix $\mathbf{C}$ was obtained by considering the definition of quantity $\langle D_3 \rangle$ in Eq. (6) for the 2D hydrostatic case.

3.2 High frequency applications

In ultrasonic applications, thin plates of the piezocomposite are excited near their thickness-mode resonance. In this case, the quantity that describes the performance of the ultrasonic transducer is (see Smith and Auld 1991):

- Electromechanical Coupling Factor (k_t)

$$k_t = \sqrt{\frac{e_{33}^2}{c_{33}^D \epsilon_{33}^S}} \tag{14}$$

where the properties are defined in Eq. (5) and $c_{33}^D = c_{33}^E + (e_{33})^2/\epsilon_{33}^S$.

In addition to k_t, two other quantities are of interest for ultrasonic transducers in ultrasonic imaging: acoustic impedance ($Z = \sqrt{c_{33}^D}\rho$) and longitudinal velocity ($v_t = \sqrt{c_{33}^D/\rho}$, where ρ is the composite density). In order to increase the performance of the transducer, we must try to maximize k_t and minimize the acoustic impedance Z. A low acoustic impedance guarantees good coupling between the transducer and the external medium (usually water or a water-like medium). In addition, in order to model the composite as a homogeneous medium, the wavelength (λ) must be much larger than the dimension of the piezocomposite microstructure. Therefore, considering the relation $v_t = \lambda f$, where f is the specified operation frequency of the transducer, the longitudinal velocity v_t must be kept high, otherwise it causes a reduction of λ (see Smith and

Auld 1991). The definitions of k_t, Z, and v_t do not change for the 2D plane strain case.

4
Homogenization in piezoelectricity

In this section, a brief introduction to the theory of the homogenization method applied to piezoelectricity is presented. Homogenization allows the calculation of the effective properties of a complex periodic material (see Sanches and Sances 1992). Periodic materials are composed of a periodic repetition of unit cells. The homogenization theory applied to piezoelectricity was developed by Telega (1990), and Galka et al. (1992). The numerical implementation of the theory is discussed and homogenization is compared with differential effective medium theory (DEM).

4.1
Theoretical formulation

Considering the standard homogenization procedure, the unit cell is defined as $Y = [0, Y_1] \times [0, Y_2] \times [0, Y_3]$ and let the material functions c^E_{ijkl}, e_{ijk}, and ϵ^S_{ij} be Y-periodic functions:

$$\begin{aligned}
&\mathbf{C}^{E\varepsilon}(\mathbf{x}) = \mathbf{C}^E(\mathbf{x}, \mathbf{y}); \;\; \mathbf{e}^{\varepsilon}(x) = \mathbf{e}(\mathbf{x}, \mathbf{y}); \;\; \boldsymbol{\epsilon}^{S\varepsilon}(\mathbf{x}) = \boldsymbol{\epsilon}^S(\mathbf{x}, \mathbf{y}) \\
&\mathbf{C}^{E\varepsilon}(\mathbf{x}, \mathbf{y}) = \mathbf{C}^E(\mathbf{x}, \mathbf{y} + \mathbf{Y}); \;\; \mathbf{e}^{\varepsilon}(\mathbf{x}, \mathbf{y}) = \mathbf{e}(\mathbf{x}, \mathbf{y} + \mathbf{Y}); \\
&\boldsymbol{\epsilon}^{S\varepsilon}(\mathbf{x}, \mathbf{y}) = \boldsymbol{\epsilon}^S(\mathbf{x}, \mathbf{y} + \mathbf{Y})
\end{aligned} \tag{15}$$

and $\mathbf{y} = \mathbf{x}/\varepsilon$ where $\varepsilon > 0$ is a parameter with small value which represents the microscale in which the properties are changing (composite microstructure scale).

Expanding $\mathbf{u}$ and ϕ asymptotically, we get (see Telega 1990):

$$\begin{aligned}
&\mathbf{u}^{\varepsilon} = \mathbf{u}_0(\mathbf{x}) + \varepsilon \mathbf{u}_1(\mathbf{x}, \mathbf{y}) \\
&\phi^{\varepsilon} = \phi_0(\mathbf{x}) + \varepsilon \phi_1(\mathbf{x}, \mathbf{y})
\end{aligned} \tag{16}$$

where only the first order variation terms were considered and $\mathbf{u}_1$ and ϕ_1 are Y-periodic.

Equations (16) and properties (15) must be substituted into the energy functional for the piezoelectric medium given by the expression (see Tiersten 1967):

$$\begin{aligned}
G(\mathbf{v}, \varphi) = &\frac{1}{2}\int_\Omega \boldsymbol{\varepsilon} : \mathbf{C}^E : \boldsymbol{\varepsilon} \mathrm{d}\Omega - \frac{1}{2}\int_\Omega \nabla\varphi \epsilon^S \nabla\varphi \mathrm{d}\Omega \\
&+ \int_\Omega \boldsymbol{\varepsilon} : \mathbf{e}\nabla\varphi \mathrm{d}\Omega - \int_\Omega \mathbf{v}\mathbf{b}\mathrm{d}\Omega - \int_\Gamma \mathbf{v}\mathbf{t}\mathrm{d}\Omega \\
&+ \int_\Gamma \varphi \mathbf{d} \mathrm{d}\Omega
\end{aligned} \tag{17}$$

where $\boldsymbol{\varepsilon}$ is the mechanical strain, $\nabla\varphi$ the electrical gradient, $\mathbf{b}$ the body forces, $\mathbf{t}$ the surface traction and $\mathbf{d}$ the surface electrical charges. $\mathbf{C}^E, \boldsymbol{\epsilon}^S$, and $\mathbf{e}$ were defined in Eq. (5).

After the substitution and application of the theory of asymptotic analysis (see Sanches and Sanches 1992), we can extract the macroscopic and microscopic equations. Due to the linearity of the problem we can assume that (see Galka et al. 1992):

$$\begin{aligned}
&\mathbf{u}_1 = \boldsymbol{\chi}(\mathbf{x}, \mathbf{y})\boldsymbol{\varepsilon}(\mathbf{u}_0(\mathbf{x})) + \boldsymbol{\Phi}(\mathbf{x}, \mathbf{y})\nabla\phi_0(\mathbf{x}) \\
&\phi_1 = \psi(\mathbf{x}, \mathbf{y})\boldsymbol{\varepsilon}(\mathbf{u}_0(\mathbf{x})) + R(\mathbf{x}, \mathbf{y})\nabla\phi_0(\mathbf{x})
\end{aligned} \tag{18}$$

where $\boldsymbol{\chi}(\mathbf{x}, \mathbf{y})$ is the characteristic displacement of the unit cell, $R(\mathbf{x}, \mathbf{y})$ is the characteristic electric potential of the unit cell, and $\psi(\mathbf{x}, \mathbf{y})$ and $\boldsymbol{\Phi}(\mathbf{x}, \mathbf{y})$ are the characteristic "coupled" functions of the unit cell. All of these functions are Y-periodic; $\boldsymbol{\chi}(\mathbf{x}, \mathbf{y})$ and $\boldsymbol{\Phi}(\mathbf{x}, \mathbf{y})$ belong to $H_{per}(Y, R^3)$, and $\psi(\mathbf{x}, \mathbf{y})$ and $R(\mathbf{x}, \mathbf{y})$ belong to $H_{per}(Y)$, where: $H_{per}(Y) = \{v \in H^1(Y) \mid v$ takes equal values on opposite sides of Y$\}$, $H_{per}(Y, R^3) = \{\boldsymbol{v} = (v_i) \mid v_i \in H_{per}(Y), i = 1, 2, 3\}$ which corresponds to the periodicity condition in the unit cell.

Substituting (18) into the microscopic equation and seeking its solution, we obtain two sets of equations (see Telega 1990, and Galka et al. 1992):

$$\int_Y \left[c_{ijkl}(\boldsymbol{x}, \boldsymbol{y}) \left(\delta_{im}\delta_{jn} + \frac{\partial \chi_i^{(mn)}}{\partial y_j} \right) + e_{ikl}(\boldsymbol{x}, \boldsymbol{y}) \frac{\partial \psi^{(mn)}}{\partial y_i} \right] \varepsilon_{kl}(\mathbf{v}) \mathrm{d}Y = 0, \;\; \forall \mathbf{v} \in H_{per}(Y, R^3) \tag{19}$$

$$\int_Y \left[e_{kij}(\boldsymbol{x}, \boldsymbol{y}) \left(\delta_{im}\delta_{jn} + \frac{\partial \chi_i^{(mn)}}{\partial y_j} \right) - \epsilon_{ik}(\boldsymbol{x}, \boldsymbol{y}) \frac{\partial \psi^{(mn)}}{\partial y_i} \right] \frac{\partial w}{\partial y_k} \mathrm{d}Y = 0, \forall \; w \in H_{per}(Y) \tag{20}$$

$$\int_Y \left[c_{klij}(\boldsymbol{x}, \boldsymbol{y}) \frac{\partial \Phi_k^{(m)}}{\partial y_l} + e_{kij}(\boldsymbol{x}, \boldsymbol{y}) \left(\delta_{mk} + \frac{\partial R^{(m)}}{\partial y_k} \right) \right] \varepsilon_{ij}(\mathbf{v}) \mathrm{d}Y = 0, \;\; \forall \mathbf{v} \in H_{per}(Y, R^3) \tag{21}$$

$$\int_Y \left[e_{kij}(\boldsymbol{x}, \boldsymbol{y}) \frac{\partial \Phi_i^{(m)}}{\partial y_j} - \epsilon_{ik}(\boldsymbol{x}, \boldsymbol{y}) \left(\delta_{mi} + \frac{\partial R^{(m)}}{\partial y_i} \right) \right] \frac{\partial w}{\partial y_k} \mathrm{d}Y = 0, \;\; \forall w \in H_{per}(Y) \tag{22}$$

Having solved these local problems, we can determine the homogenized properties. They are given by (see Telega 1990, and Galka et al. 1992):

$$\begin{aligned}
c^h_{rspq}(\boldsymbol{x}) = &\frac{1}{\mid Y \mid} \left\{ \int_Y \left[c_{ijkl}(\boldsymbol{x}, \boldsymbol{y}) \left(\delta_{ip}\delta_{jq} + \frac{\partial \chi_i^{(pq)}}{\partial y_j} \right) \right. \right. \\
&\times \left(\delta_{kr}\delta_{ls} + \frac{\partial \chi_k^{(rs)}}{\partial y_l} \right) \\
&\left. \left. + e_{kij}(\boldsymbol{x}, \boldsymbol{y}) \left(\delta_{ip}\delta_{jq} + \frac{\partial \chi_i^{(pq)}}{\partial y_j} \right) \frac{\partial \psi^{(rs)}}{\partial y_k} \right] \mathrm{d}Y \right\}
\end{aligned} \tag{23}$$

$$\begin{aligned}
e^h_{prs}(\boldsymbol{x}) = &\frac{1}{\mid Y \mid} \left\{ \int_Y \left[e_{kij}(\boldsymbol{x}, \boldsymbol{y}) \left(\delta_{kp} + \frac{\partial R^{(p)}}{\partial y_k} \right) \right. \right. \\
&\left. \left. (\delta_{ir}\delta_{js} + \frac{\partial \chi_i^{(rs)}}{\partial y_j}) - .e_{kij}(\boldsymbol{x}, \boldsymbol{y}) \frac{\partial \Phi_i^{(p)}}{\partial y_j} \frac{\partial \psi^{(rs)}}{\partial y_k} \right] \mathrm{d}Y \right\}
\end{aligned} \tag{24}$$

$$\epsilon^h_{pq}(\boldsymbol{x}) = \frac{1}{|Y|}\left\{\int_Y \left[\epsilon_{ij}(\boldsymbol{x},\boldsymbol{y})\left(\delta_{ip}+\frac{\partial R^{(p)}}{\partial y_i}\right)\left(\delta_{jq}+\frac{\partial R^{(q)}}{\partial y_j}\right) - e_{kij}(\boldsymbol{x},\boldsymbol{y})\left(\delta_{kp}+\frac{\partial R^{(p)}}{\partial y_k}\right)\frac{\partial \Phi^{(q)}_i}{\partial y_j}\right] \mathrm{d}Y\right\} \quad (25)$$

and $c^h_{ijkl} = c^h_{klij} = c^h_{jikl}$, $e^h_{ijk} = e^h_{ikj}$, $\epsilon^h_{ij} = \epsilon^h_{ji}$.

4.2
Numerical implementation

The previous equations have an analytical solution only for simple cases (such as the one-dimensional unit cell). For unit cells with complex topologies a solution can be obtained using the finite element method (FEM). In FEM, the base cell is discretized by N finite elements, and the integrals (19), (20), (21), (22), (23), (24), and (25) are transformed in a summation of integrals over each finite element. Four-node bilinear elements were used in the implementation. Essentially, for the 2D case, there are three load cases to be solved in Eqs. (19) and (20) (indices mn are 11, 33, and 13 or 31), and two load cases in Eqs. (21) and (22) (index m is 1 and 3). For the 3D problem, there are six load cases to be solved in Eqs. (19) and (20) (indices mn are 11, 22, 33, 12 or 21, 23, or 32, and 13 or 31), and three load cases in Eqs. (21) and (22) (index m is 1, 2, and 3).

The displacements and electric potential of some point of the cell must be prescribed to overcome the non-unique solution of the problem, otherwise the problem will be ill posed. The choice of the point or the prescribed values does not affect the homogenized coefficients, since we only use derivatives of the characteristic functions in their computation (see Fonseca and Kikuchi 1995).

The computational implementation of the homogenization algorithm can be obtained adapting a standard finite element code applied to piezoelectricity (see Naillon et al. 1983).

4.3
Symmetry considerations

If the piezocomposite cell has some kind of symmetry in relation to axes or planes, we can take advantage of this in order to reduce the computational cost. In this case, optimization and homogenization are conducted only in one part of the domain. If the cell is symmetric in relation to one or two axes in the 2D plane strain case (or planes in the 3D problem) the homogenized coefficients will be at least orthotropic, since the piezoelectric material is orthotropic and must be present in the unit cell. If there is no symmetry at all, the homogenized coefficients will be anisotropic. If the piezocomposite is orthotropic, the number of independent homogenized coefficients is reduced to four elastic coefficients for the 2D case and nine for the 3D case, and the number of dielectric coefficients is reduced to two for the 2D case and three for the 3D case. The piezoelectric homogenized coefficients depend on the kind of crystal class considered for the basic piezoelectric material. For the 4 *mm* tetragonal class considered in this work, there are three piezoelectric coefficients for the 2D case and four in the 3D case.

The symmetry conditions applied in the homogenization calculations in the 2D plane strain case are presented in appendix A.

4.4
Comparison with other methods

There are other methods for calculating effective properties of piezocomposite materials. The main advantage of the homogenization method presented here, in relation to other methods, is that it is not limited by the shape of the inclusions and matrix that make the composite unit cell. Other method, such as the differential effective medium theory (DEM) presented in Avellaneda and Swart (1994) would not be applicable in our work, since the DEM cannot treat unit cells with complex topologies.

However, in order to verify the accuracy of the homogenization method for piezoelectricity, we compare its results with the results of the differential effective medium theory (DEM) for a simple unit cell topology. The DEM evaluates the piezocomposite effective properties for all volume fractions and is exact in the small volume fraction limit (see Avellaneda and Swart 1994). The unit cell considered is shown in Fig. 1. In Figs. 2, 3, 4 and 5 coefficients d_h, $d_h g_h$, and k_h are plotted as a function of the ceramic

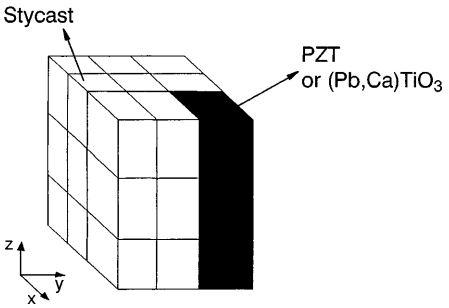

Fig. 1. Composite unit cell discretized by a $3 \times 3 \times 3$ finite element mesh

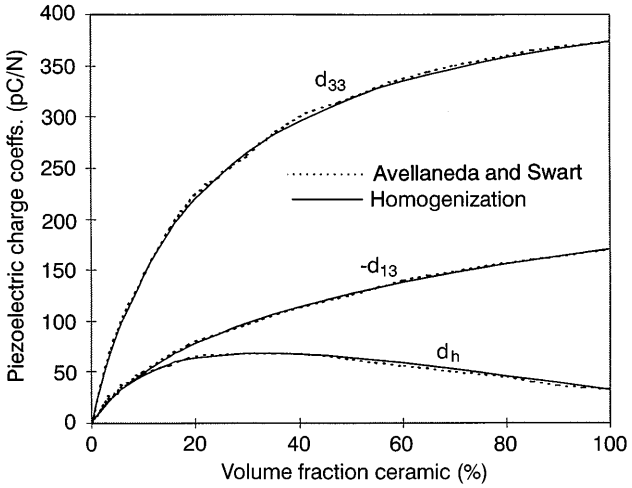

Fig. 2. Comparison among composite piezoelectric charge coefficients d_{13}, d_{33}, and d_h obtained using DEM and homogenization, as a function of piezoceramic volume fraction for a PZT5A/Stycast composite

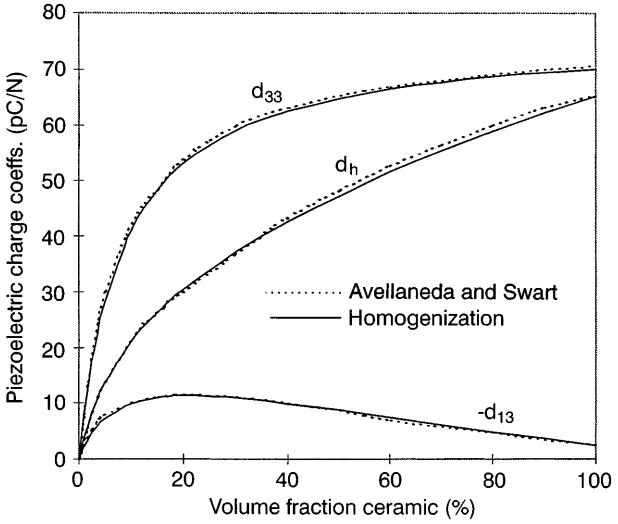

Fig. 3. Comparison among composite piezoelectric charge coefficients d_{13}, d_{33}, and d_h obtained using DEM and homogenization, as a function of piezoceramic volume fraction for a (Pb,Ca)TiO_3/Stycast composite

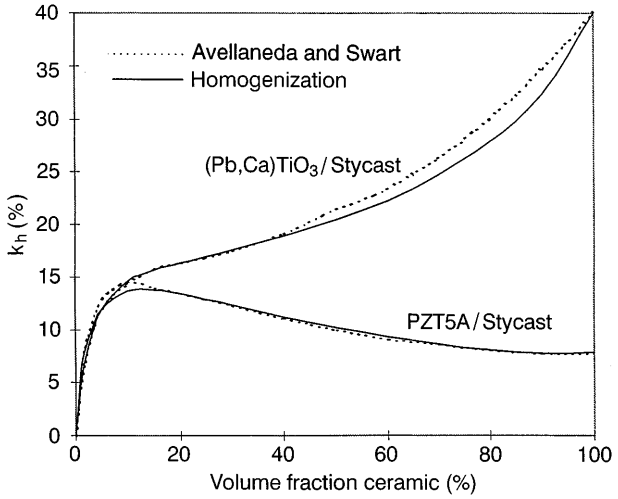

Fig. 5. Comparison among composite hydrostatic electromechanical coupling factor k_h obtained using DEM and homogenization, as a function of piezoceramic volume fraction

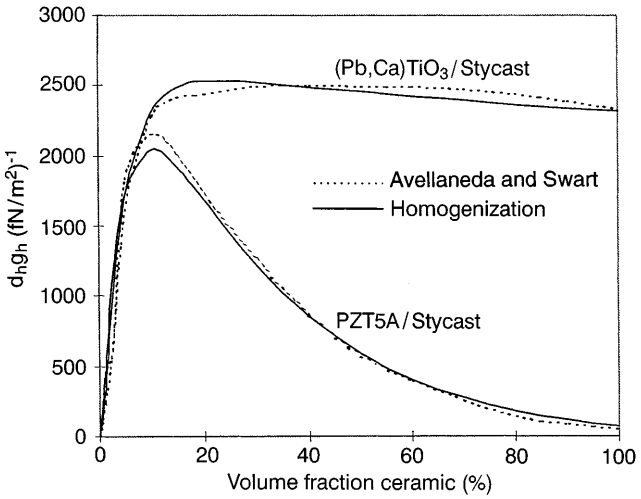

Fig. 4. Comparison among composite hydrostatic figure of merit $d_h g_h$ obtained using DEM and homogenization, as a function of piezoceramic volume fraction for a (Pb,Ca)TiO_3/Stycast and PZT5A/Stycast composites

Table 1. Material Properties of PZT5, (Pb, Ca) TiO_3 and Stycast

Piezoceramic	PZT5	(Pb, Ca)TiO_3
c_{11}^E (10^{10} N/m^2)	12.04	15.05
c_{12}^E (10^{10} N/m^2)	7.52	3.68
c_{13}^E (10^{10} N/m^2)	7.51	3.09
c_{33}^E (10^{10} N/m^2)	11.09	12.78
c_{44}^E (10^{10} N/m^2)	2.3	1.20
c_{66}^E (10^{10} N/m^2)	2.1	1.14
e_{13} (C/m^2)	−5.4	1.71
e_{33} (C/m^2)	15.8	8.8
e_{15} (C/m^2)	12.3	0.33
$\epsilon_{11}^S/\epsilon_0$	540	170
$\epsilon_{33}^S/\epsilon_0$	830	140
Polymer	Stycast	
c_{11} (10^{10} N/m^2)	1.23	
c_{12} (10^{10} N/m^2)	0.52	
ϵ_{33}/ϵ_0	4	

volume fraction for piezocomposites made of PZT5A/Stycast, and (Pb, Ca) TiO_3/Stycast. The properties of these materials are listed in Table 1. One can see that homogenization agrees very well with their method.

5 Topology optimization procedure

This section describes the numerical procedure for topology optimization of piezoelectric microstructures in two dimensions and discusses its numerical implementation. The procedure presented here is based on the topology optimization procedure applied to the design of elastic microstructures using the homogenization method, as described in Fonseca and Kikuchi (1996), and Sigmund (1995).

5.1 Formulation of the optimization problem

The initial domain is discretized by finite elements where the design variables are the amount of material (x) in each finite element. The objective is to maximize one of the performance characteristics of the piezoelectric material presented in section 3 (defined in terms of the homogenized properties of the piezocomposite) such as the hydrostatic coupling coefficient (d_h), hydrostatic figure of merit $(d_h g_h)$, electromechanical coupling factor (k_h), or thickness mode electromechanical coupling factor (k_t), which were redefined for the 2D plane strain case. The optimization procedure is iterative and consists of the following steps (see Fig. 6): first, the effective properties of the microstructure are obtained by using the homogeni-

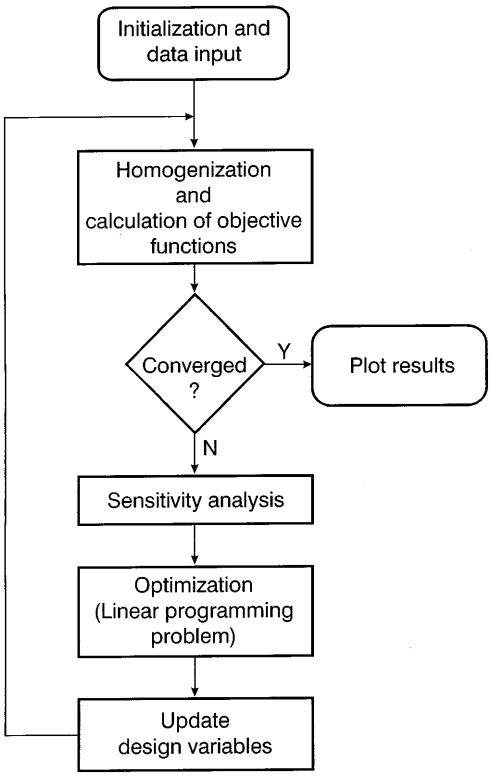

Fig. 6. Flowchart of the optimization procedure

zation method so the performance characteristics can be calculated. Then, using an optimization algorithm (such as linear programming method), a new distribution of material that maximizes the performance is obtained. This procedure is repeated and the iteration proceeds until convergence is obtained.

5.1.1 Element material properties

In this work, the material properties in a given element is simply some fraction x times the material properties of the basic material. This is an "artificial" material model for intermediate densities, but since we obtain an entirely solid material or void in each element, this is a valid approach. However, during the optimization process intermediate densities are allowed and consist of artificial (nonexisting) materials. By using this model the design procedure is greatly simplified (see Sigmund and Torquato 1996).

The basic material has stiffness tensor c^0_{ijkl}, piezoelectric tensor e^0_{ijk}, and dielectric tensor ϵ^0_{ij}. If the basic material considered in the analysis is the polymer (isotropic), the piezoelectric coefficients are zero. Therefore, the local tensor properties in each element n can be expressed in terms of one design variable x_n times the basic material property:

$$c^n_{ijkl} = x_n c^0_{ijkl} \quad e^n_{ijk} = x_n e^0_{ijk} \quad \epsilon^n_{ij} = x_n \epsilon^0_{ij} \tag{26}$$

where x_n represents the amount of basic material in that element (local density) that ranges from $x_{\min}$ to 1. For $x_n = x_{\min}$ the element is a "void" and for $x_n = 1$ the element is a solid material.

Considering that the design domain was discretized in N finite elements, the material type will change from element to element during the optimization. The design problem consists of finding the fraction x_n amount of material in each element such that the objective function is maximized or minimized.

5.1.2 Constraints

The maximization of the piezoelectric response can be reached allowing a decrease in the effective stiffness of the composite material. One can try to give a physical explanation for this considering the nature of the piezoelectric effect. Essentially, this effect occurs due to Coulomb forces that try to deform the material elastic matrix. These Coulomb forces appear due to the presence of dipoles in the material molecule (Ristic 1983). In order to maximize the piezoelectric response (usually strain) we must expect a decrease in the stiffness of the matrix. This was verified numerically in the optimization.

Lower stiffness is undesirable, therefore, a lower bound constraint on effective stiffness should be specified. Since the microstructure is orthotropic, we must choose a stiffness coefficient for the constraint $(c_{\min})$. The decision of which stiffness coefficient should be constrained depends on the problem, as will be discussed later in the results section.

A lower bound $x_{\min}$ is also specified for the design variables x_n to avoid numerical problems (singularity of the stiffness matrix in the finite element formulation). In this work $x_{\min}$ was chosen to be 10^{-4}. Numerically, regions with $x_n = x_{\min}$ have practically no structural significance and can be considered void regions. Therefore, the bounds for the design variable are $0 < x_{\min} \leq x_n \leq 1$ (see Sigmund and Torquato 1996).

Another constraint is related to the symmetry conditions imposed. As the expected composite material is necessarily orthotropic (since the basic piezoelectric material is orthotropic), two kinds of symmetry can be defined in the microstructure domain for the 2D plane strain case: one in relation to the horizontal axis and the other in relation to both axes. The symmetry conditions are implicitly expressed in the boundary conditions during the homogenization, as stated in appendix A. In this work no volume constraint was specified.

Considering all these features, the final optimization problem can be stated as:

$$\begin{aligned} \text{Maximize} \quad & : F(\mathbf{x}), \text{where } \mathbf{x} = [x_1, x_2, \ldots, x_n, \ldots, x_N] \\ \text{subject to} \quad & : c_{ijkl} \geq c_{\min}, i, j, k, l \text{ are specified values} \\ & \quad 0 < x_{\min} \leq x_n \leq 1 \end{aligned}$$

where x_n is the design variable on the n-th element and $F(\mathbf{x})$ is the performance characteristic to be maximized.

5.2 Optimization method

In this work, as we are considering several different objective functions and some constraints, we decided to use the mathematical programming method called sequence linear programming (SLP). This method consists of the

sequential solution of approximate linear subproblems that can be defined writing Taylor series expansion for the objective and constraints functions around the current design point x_n in each iteration step. This method has been successfully used in the design of microstructures (see Fonseca and Kikuchi 1996 and Sigmund and Torquato 1996).

The linearization of the problem (Taylor series) requires the sensitivities (gradients) of the objective function and constraints in relation to x_n. These sensitivities can be expressed as a function of the sensitivities of the material coefficients derived in appendix B. Contrary to the design of elastic microstructures, where the gradients can be easily obtained analytically, in the piezoelectric case, we could not obtain a simplified expression. Therefore, the solution of an additional finite element problem is required for the gradient calculation, making it computationally expensive.

In the SLP solution we apply the moving-limits strategy to stabilize the process convergence (see Fonseca and Kikuchi 1996). The rule used is that the change in the moving-limits of the design variables is reduced when the change in the objective function starts to decrease during three consecutive iterations (close to convergence). The changes in the moving-limits can be specified as percentages.

5.3
Numerical implementation

A flowchart of the optimization algorithm describing the steps involved is shown in Fig. 6. The software was implemented in FORTRAN language.

A random distribution of material is used as a starting guess. A lot of computer time can be saved if the starting guess is close to the optimal topology. However, we usually do not know the optimal topology, so in order to overcome this problem the result obtained with a coarse mesh (10×10) is transferred to a refined mesh (20×20) and it is used as an initial guess for the calculations in the refined mesh. This provides significant savings in the computational time for the refined mesh and helps to verify the convergence of the solution. The result of the coarse mesh can be considered a good initial guess for the refined mesh.

The equations for the homogenization and its solution were presented in section 4. The linear programming subproblem in each iteration of the SLP is solved using the package DSPLP from the SLATEC library (see Hanson and Hiebert 1981).

The iteration proceeds until the change in the objective function during three consecutive iterations is less than 10^{-4} (by experience).

6
Results

Material properties of the basic materials and the configurations used for the design are described in this section. The performance of the microstructures obtained is compared with the performance of pure piezoelectric material and a simple unit cell design.

6.1
Material properties used in the simulations

Table 2 describes the properties of the piezoceramic and polymer used in the composite. Considering 2D plane strain conditions in plane 1-3 (or xz) only the properties $c^E_{11}, c^E_{13}, c^E_{33}, c^E_{44}, e_{13}, e_{33}, e_{15}, \epsilon^S_{11}/\epsilon_0$, and $\epsilon^S_{33}/\epsilon_0$ were used for the piezoelectric material.

6.2
Optimized piezoelectric microstructures

Piezoelectric materials used in transducer design are usually ceramics (orthotropic materials) that are very difficult to fabricate with complex shapes. Therefore, two kinds of initial domains are considered. In the first model, there are two materials in the unit cell: polymer and piezoelectric materials. The polymer is the design domain and the piezoelectric domain remains unchanged during this analysis. This configuration was chosen to avoid the difficulties in manufacturing piezoceramics with complex topologies. Our goal is to obtain a unit cell that presents complex topology only in the polymer domain. In the second model the entire domain consists of piezoceramic (no polymer at all).

The initial configuration considered for the unit cell in the first model is shown in Fig. 7. The initial "volume fraction" (vol%) of ceramic was set to 20%. This volume fraction changes during the optimization procedure since material is removed from or added to the polymer domain.

Table 2. Material Properties of PZT5 and Spurr polymer

Piezoceramic	PZT5
c^E_{11} (10^{10} N/m^2)	12.1
c^E_{12} (10^{10} N/m^2)	7.54
c^E_{13} (10^{10} N/m^2)	7.52
c^E_{33} (10^{10} N/m^2)	11.1
c^E_{44} (10^{10} N/m^2)	2.30
c^E_{66} (10^{10} N/m^2)	2.10
e_{13} (C/m^2)	−5.4
e_{33} (C/m^2)	15.8
e_{15} (C/m^2)	12.3
$\epsilon^S_{11}/\epsilon_0$	1650
$\epsilon^S_{33}/\epsilon_0$	1700
Polymer	Spurr
c_{11} (10^{10} N/m^2)	0.53
c_{12} (10^{10} N/m^2)	0.31
ϵ_{33}/ϵ_0	4

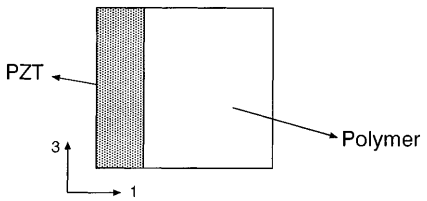

Fig. 7. Configuration for the first model. The piezoelectric domain is kept unchanged

Table 3. Performance characteristics for two basic unit cells

Unit cell	$\|d_h\|$ (pC/N)	$d_h g_h$ (pm^2/N)	k_h	k_t
PZT5 (full)	68.2	0.222	0.145	0.361
PZT5/polymer (20 vol%)	90.95	2.06	0.112	0.455

For the first model, the stiffness constraint (lower bound) is specified for coefficient c_{11}^E since it is expected that the unchanged piezoceramic domain provides enough stiffness in 3 (or z) direction. In the second case (design domain consists only of piezoelectric material) the stiffness constraint is specified for c_{11}^E, although other coefficients could have been used.

Two kinds of symmetry conditions were considered in the optimization: one in relation only to 1 (or x) axis, and the other in relation to 1 (or x) and 3 (or z) axes.

Table 3 presents the values of the performance characteristics (see section 3) considering the unit cell fully made of PZT5 material and a simple unit cell having 20% "volume fraction" of PZT5 in a polymer (effective properties obtained using homogenization). The results obtained with the proposed method will be compared with these results.

Figures 8 through 12 show microstructure topologies obtained when considering the first model configuration in the initial domain. The performance characteristics for these topologies are listed in Table 4. Symmetry conditions in 1 (or x) and 3 (or z) axes were considered.

The problem is not convex since different starting points result in different topologies that maximize the performance characteristics. The non-uniqueness of the solution is intrinsic to the mathematical formulation (for example, we could have an unlimited number of possible definitions of the unit cell of the periodic media). Figures 8 and 9 illustrate the non-uniqueness. They present topologies that maximize $|d_h|$ obtained by considering different starting points. The stiffness constraints are shown in table 4 for each case. The topology in Fig. 9 has a lower stiffness constraint giving a larger value for $|d_h|$.

Figure 10 shows a microstructure that has an optimized $d_h g_h$. Figure 11 presents a unit cell that maximizes k_h, and Fig. 12 shows one that maximizes k_t. The stiffness constraint in each case is shown in Table 4. The topology that maximizes $d_h g_h$ is very similar to the ones that maximize $|d_h|$. The optimized value obtained for $d_h g_h$ is lower than the one obtained in Fig. 9 for the same stiffness constraint showing that this may be a local maximum.

Comparing the values of Table 4 with the values in Table 3, the following improvement can be verified in relation to the simple unit cell PZT5/polymer (20 vol%): 2.7 times in $|d_h|$, 7 times in $d_h g_h$, 1.6 times in k_h, and 1.2 times in k_t. In relation to the pure piezoelectric material, there

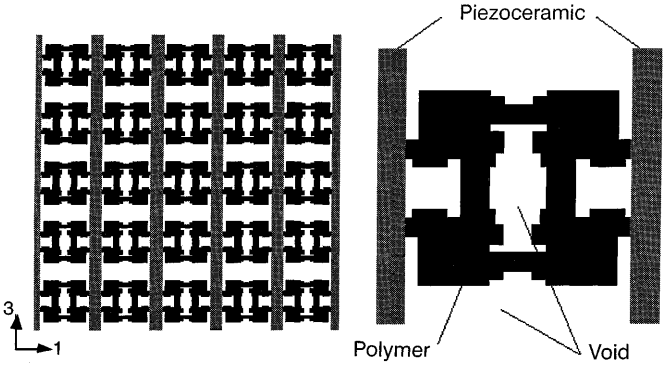

Fig. 9. Microstructure that maximizes $|d_h|$. Different initial guess than previous figure. A 20 × 20 mesh for one quarter of the cell was used

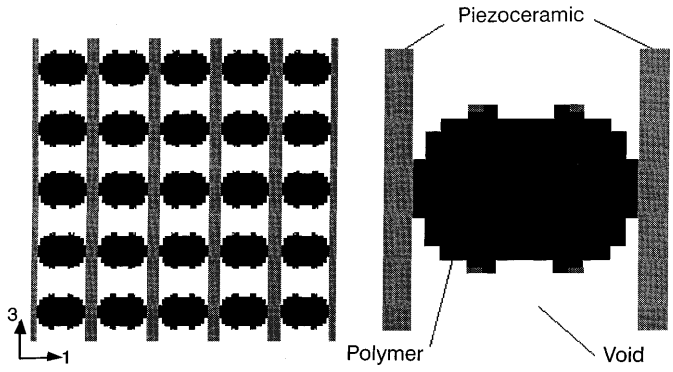

Fig. 8. Microstructure that maximizes $|d_h|$. A 20 × 20 mesh for one quarter of the cell was used

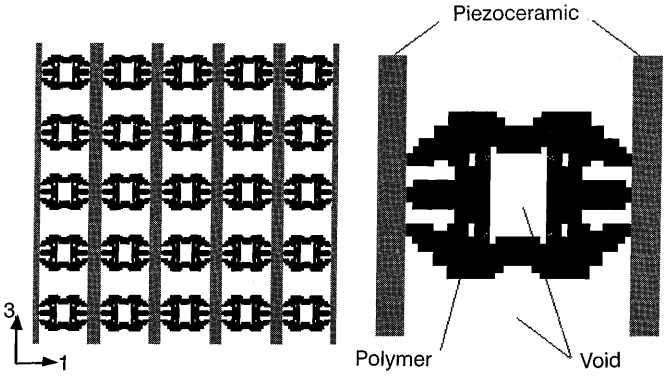

Fig. 10. Microstructure that optimizes $d_h g_h$. A 20 × 20 mesh for one quarter of the cell was used

Table 4. Performance characteristics of the unit cells described in the figs.

Fig.	Design	$c_{11}^E(10^9 N/m^2)>$	$\| d_h \|$ (pC/N)	$d_h g_h$ (pm^2/N)	k_h	k_t
8	max. $\|d_h\|$	1.4	234.0	13.1	0.13	0.52
9	max. $\|d_h\|$	0.8	253.0	15.3	0.11	0.52
10	max. $d_h g_h$	0.8	249.0	15.0	0.11	0.52
11	max. k_h	3.0	217.0	11.3	0.18	0.51
12	max. k_t	0.8	229.0	12.6	0.10	0.52

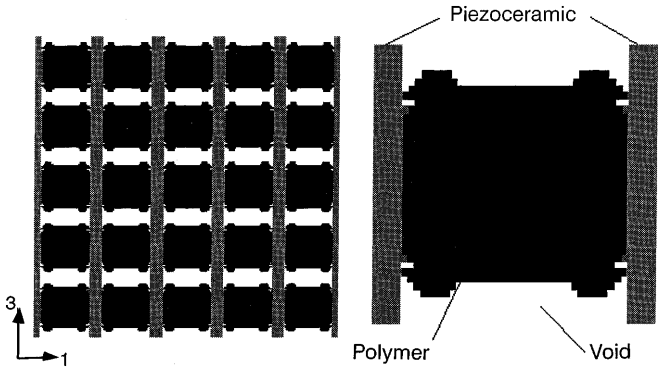

Fig. 11. Microstructure that maximizes k_h. A 20 × 20 mesh for one quarter of the cell was used

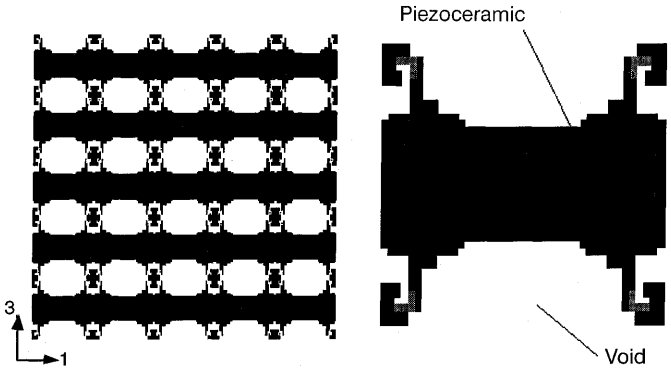

Fig. 13. Microstructure that maximizes $|d_h|$. The entire initial domain made of piezoelectric material. A 20 × 20 mesh for one quarter of the cell was used

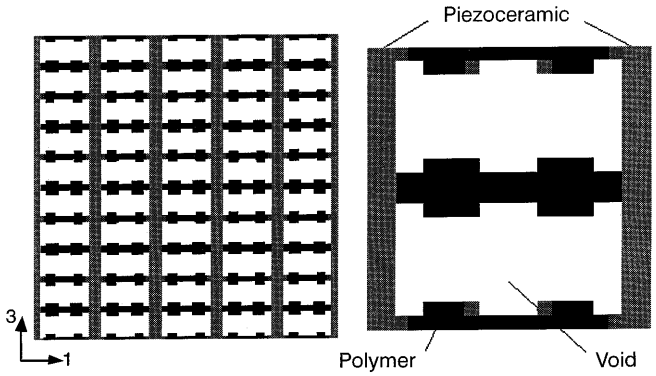

Fig. 12. Microstructure that maximizes k_t. A 10×10 mesh for one quarter of the cell was used

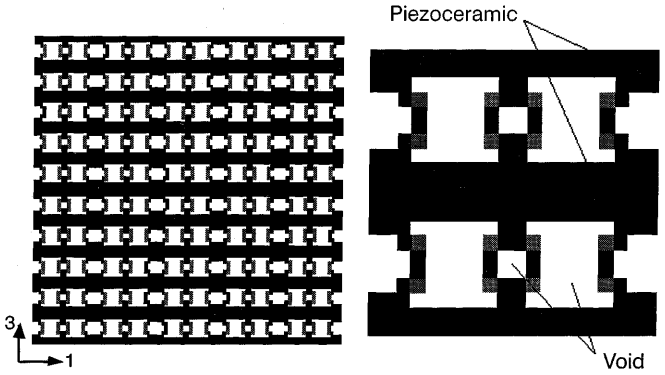

Fig. 14. Microstructure that maximizes $|d_h|$. The entire initial domain made of piezoelectric material. Different initial guess than previous figure. A 10 × 10 mesh for one quarter of the cell was used

was an improvement of 3.7 times in $|d_h|$, 69 times in $d_h g_h$, 1.2 times in k_h, and 1.4 times in k_t.

Table 5 shows the values of performance characteristics obtained considering the second model (the entire design domain made of piezoelectric material). The optimized unit cell topologies are presented in Figs. 13, 14 and 15. Symmetry conditions in 1 (or x) and 3 (or z) axes were considered. The stiffness constraint specified is shown in Table 5. Figures 13 and 14 present two different topologies that maximize $|d_h|$ obtained when using different starting points.

Comparing the values of Table 5 with the values in Table 3, the following improvement can be verified in relation to the simple unit cell PZT5/polymer (20 vol%): 3 times in $|d_h|$ and 3.7 times in k_h. In relation to the pure piezoelectric material, there was an improvement of 3.8 times in $|d_h|$ and 3 times in k_h. By specifying lower stiffness constraints, greater improvement can be achieved.

Figure 16 shows the topology that maximizes $|d_h|$ obtained by considering the first model and symmetry only in relation to 1 (or x) axis. Figure 17 presents the microstructure topology that optimizes $|d_h|$ obtained by considering the second model (only piezoelectric material in

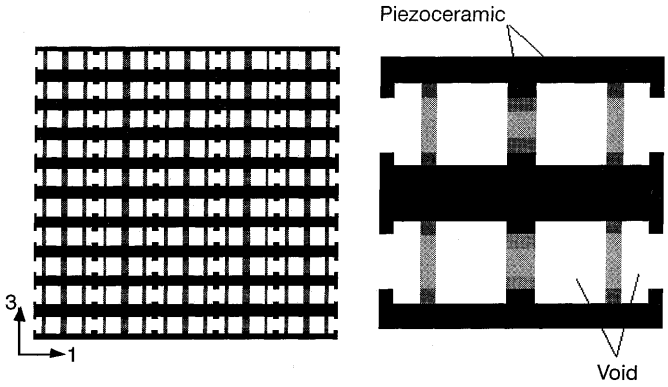

Fig. 15. Microstructure that maximizes k_h. The entire initial domain made of piezoelectric material. A 10 × 10 mesh for one quarter of the cell was used

Table 5. Performance characteristics of the unit cells described in the figures

Fig.	Design	$c_{11}^E(10^9$ N/m^2)>	$\|d_h\|$ (pC/N)	$d_h g_h$ (pm^2/N)	k_h	k_t
13	max. $\|d_h\|$	40.0	265.0	26.8	0.40	0.44
14	max. $\|d_h\|$	40.0	260.0	16.4	0.36	0.41
15	max. k_h	40.0	221.0	28.9	0.42	0.47

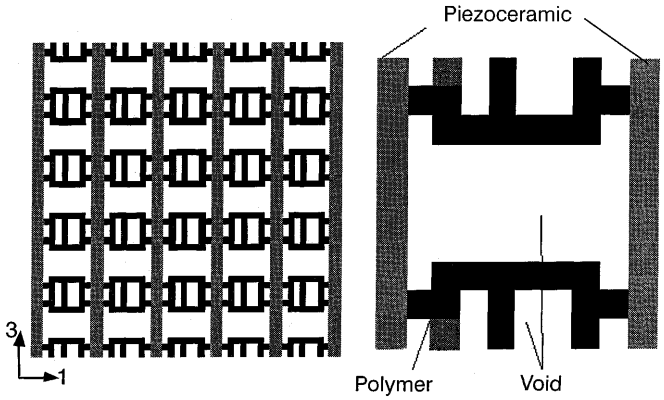

Fig. 16. Microstructure that maximizes $|d_h| = 247.0$ *p*C/N-symmetry in relation to x axis. A 10×10 mesh for the entire cell was used

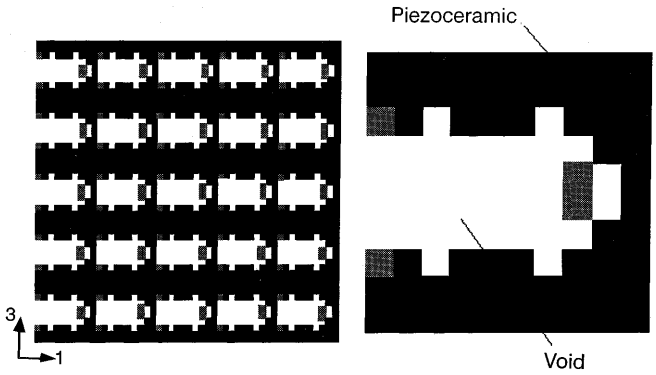

Fig. 17. Microstructure that maximizes $|d_h| = 228.0$ *p*C/N-symmetry in relation to x axis. The entire initial domain made of piezoelectric material. A 10×10 mesh for the entire cell was used

the design domain) and symmetry only in relation to x axis. A constraint in the stiffness coefficient $c_{11}^E > 8.10^8 \mathrm{N/m^2}$ was specified in each case. The same improvement was obtained as in the examples with two symmetry axes.

Figure 18 describes the change in the microstructure topology that maximizes $|d_h|$ as the stiffness constraint in coefficient c_{11}^E is decreased. The value of $|d_h|$ increases from a) to f) with the decrease in the stiffness constraint, as expected. The values of the performance characteristics are shown in Table 6 for these topologies. The value of $d_h g_h$ also increases with the decrease in the stiffness constraint.

All the results for the maximization of $|d_h|$ presented above were obtained by considering positive values of d_h, as the implementation of the SLP used in this work allows

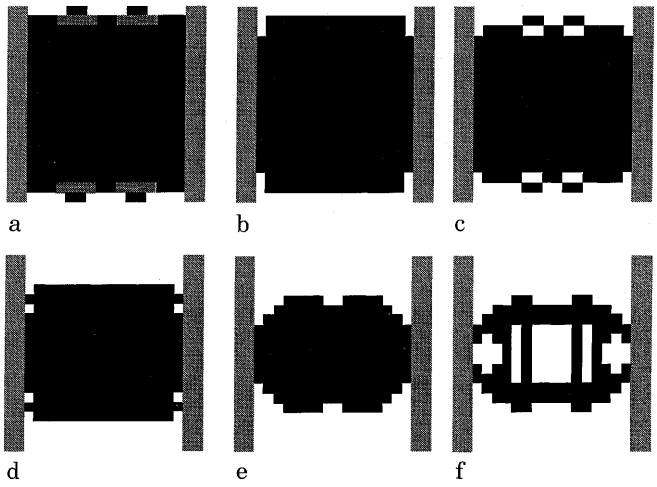

Fig. 18 a–f. Change in the microstructure topology with **a** decrease in the stiffness constraint from **a** to **f**. A 10×10 mesh for one quarter of the cell was used

only for positive values of the objective function. However, we can look for an optimal value by considering negative values. In order to verify the accuracy of the results, the homogenized properties were calculated again by considering a twice fine mesh (40 × 40 for one quarter of the cell). The results showed an average difference of 2%.

7 Conclusions

A method for designing piezoelectric microstructures with high performance characteristics using topology optimization techniques and homogenization method has been proposed. This method was implemented considering 2D plane strain microstructures. The optimization procedure determines the distribution of two phases (one material phase and one void phase) in the composite unit cell that maximize the composite performance characteristics. Two different models were considered for the optimization. In the first one, the design domain is made of polymer and the piezoelectric material remains unchanged during the analysis. In the second one, the entire domain consists of piezoceramic (no polymer at all).

Due to the importance of the homogenization method in the proposed optimization procedure, its application in the calculation of the effective properties of piezocomposite materials is described. The homogenization results were compared with the differential effective medium theory results presented in Avellaneda and Swart (1994) and very good agreement was observed.

The new microstructures obtained showed a large improvement in the performance characteristics in relation

Table 6. Performance characteristics of the unit cells described in Fig. 18

Fig.	Design	$c_{11}^E(10^9\ \mathrm{N/m^2})>$	$\lvert d_h \rvert$ (*p*C/N)	$d_h g_h$ (*p*m^2/N)	k_h	k_t
a)	max. $\lvert d_h \rvert$	4.5	163.0	6.5	0.16	0.50
b)	max. $\lvert d_h \rvert$	4.0	198.0	9.4	0.18	0.50
c)	max. $\lvert d_h \rvert$	3.5	205.0	10.1	0.18	0.51
d)	max. $\lvert d_h \rvert$	3.0	217.0	11.3	0.17	0.51
e)	max. $\lvert d_h \rvert$	2.0	228.0	12.5	0.15	0.52
f)	max. $\lvert d_h \rvert$	0.82	245.0	14.3	0.11	0.52

to the pure piezoelectric material and simple designs of piezocomposite unit cells (see Fig. 7). However, the maximization of these quantities implies a reduction in stiffness. Therefore, there is a trade-off between the maximization of the piezocomposite performance and decrease in stiffness.

The manufacture of these microstructures (even simple prototypes) is a problem that remains to be solved. Currently, most manufacturing techniques available for building complex topologies deal with ductile materials such as metals and polymers. The fragile behavior of piezoceramic makes it inappropriate for building complex shapes. In this sense, the first model presented seeks an approach that makes the manufacturing of the unit cell easier.

In future work, a filter for the optimization that avoids possible checkerboards and hinges defined by one-node contact between elements (Fonseca and Kikuchi 1996) will be implemented. A multiobjective function using weights may also be considered in the simultaneous optimization of all performance characteristics. For high frequency applications, a multiobjective function including k_t, impedance (Z), and longitudinal velocity (v_t) will be implemented. Although symmetry conditions were used in this work, no symmetry at all (anisotropic unit cells) may lead to additional improvements. Finally, the method presented in this paper will be extended to 3D microstructures (a dramatic increase in computer time is expected).

Appendix

A
Symmetry conditions for homogenization

In this appendix, we present the symmetry conditions for characteristic functions $\boldsymbol{\chi}, \boldsymbol{\Phi}$ (displacements) and ψ, R (electric potentials) (see Eq. (18)) imposed on the finite element model. These conditions allow to solve the homogenization equations considering one quarter of the unit cell (the cell is supposed to be symmetric in relation x and z axes – see Fig. 19).

In the 2D plane strain analysis there are five load cases to be solved in the homogenization problem (see section 4.2). For each of them, we present the symmetry conditions for the characteristic functions (displacements and electric potential). These conditions can be obtained by analyzing Eqs. (23), (24), and (25). We define u (displacement in x direction), w (displacement in z direction), and ϕ (electric potential). Therefore:

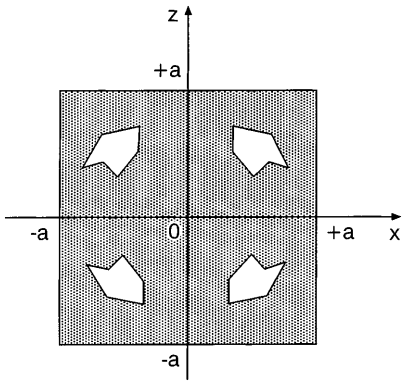

Fig. 19. Unit cell with symmetry in x and z axes

- Load Cases 1 and 2 (indices mn are 11 and 33 in Eqs. (19) and (20)):

  In $x = a$ and $x = 0 \Rightarrow u = 0$ and $\partial\phi/\partial x = 0$
  In $z = a$ and $z = 0 \Rightarrow w = 0$ and $\phi = 0$

- Load Case 3 (indices mn are 13 or 31 in Eqs. (19) and (20)):

  In $x = a$ and $x = 0 \Rightarrow w = 0$ and $\phi = 0$
  In $z = a$ and $z = 0 \Rightarrow u = 0$ and $\partial\phi/\partial z = 0$

- Load Case 4 (index m is 1 in Eqs. (21) and (22)):

  In $x = a$ and $x = 0 \Rightarrow w = 0$ and $\phi = 0$
  In $z = a$ and $z = 0 \Rightarrow u = 0$ and $\partial\phi/\partial z = 0$

- Load Case 5 (index m is 3 in Eqs. (21) and (22)):

  In $x = a$ and $x = 0 \Rightarrow u = 0$ and $\partial\phi/\partial x = 0$
  In $z = a$ and $z = 0 \Rightarrow w = 0$ and $\phi = 0$

B
Sensitivity Analysis

B.1
Sensitivity of the material coefficients

The sensitivity analysis of the material coefficients gives the gradients for the optimization procedure. The gradients allow the optimization method to make decisions about which direction to go during the optimization. In the topology design of elastic microstructures the gradient are a linear function of the mutual energies (see Fonseca and Kikuchi 1995) obtained during the homogenization process. Therefore, calculation of them is straightforward and fast (low computational cost) which contributes to increase the efficiency of the optimization. However, for the piezoelectric case the gradients cannot be easily obtained, as it will be shown in the following expressions. The calculation of them is not straightforward, having high computational cost. The semi-analytical method presented is faster than finite difference method.

The calculation of the material coefficient sensitivities starts with the derivation of Eqs. (23), (24), and (25) in relation to design variable x_n. Here, the final expressions are presented separately for each kind of property:

- Sensitivity of Elastic Properties

Deriving Eq. (23) in relation to design variable x_n and considering Eqs. (19) and (20), we get after some algebra manipulation:

$$\frac{\partial c^h_{rspq}(\boldsymbol{x})}{\partial x_n} = \frac{1}{|Y|}\left\{\int_Y \left[\frac{\partial c_{ijkl}(\boldsymbol{x},\boldsymbol{y})}{\partial x_n}\left(\delta_{ip}\delta_{jq} + \frac{\partial \chi_i^{pq}}{\partial y_j}\right)\left(\delta_{kr}\delta_{ls} + \frac{\partial \chi_k^{(rs)}}{\partial y_l}\right) + \frac{\partial e_{kij}(\boldsymbol{x},\boldsymbol{y})}{\partial x_n}\left(\delta_{ip}\delta_{jq} + \frac{\partial \chi_i^{(pq)}}{\partial y_j}\right)\frac{\partial \psi^{(rs)}}{\partial y_k}\right.\right.$$

$$+\frac{\partial^2\chi_k^{(rs)}}{\partial y_l\partial x_n}c_{ijkl}(\boldsymbol{x},\boldsymbol{y})\left(\delta_{ip}\delta_{jq}+\frac{\partial\chi_i^{(pq)}}{\partial y_j}\right)$$
$$+\frac{\partial^2\psi^{(rs)}}{\partial y_k\partial x_n}e_{kij}(\boldsymbol{x},\boldsymbol{y})\left(\delta_{ip}\delta_{jq}+\frac{\partial\chi_i^{(pq)}}{\delta y_j}\right)\Bigg]\mathrm{d}Y\Bigg\} \quad (27)$$

- Sensitivity of Piezoelectric Properties

Deriving Eq. (24) in relation to design variable x_n and considering Eqs. (19), (20), (21), and (22), we get after some algebra manipulation:

$$\frac{\partial e_{prs}^h(\boldsymbol{x})}{\partial x_n}=$$
$$\frac{1}{|Y|}\Bigg\{\int_Y\Bigg[\frac{\partial e_{kij}(\boldsymbol{x},\boldsymbol{y})}{\partial x_n}\left(\delta_{kp}+\frac{\partial R^{(p)}}{\partial y_k}\right)\left(\delta_{ir}\delta_{js}+\frac{\partial\chi_i^{(rs)}}{\partial y_j}\right)$$
$$-\frac{\partial\epsilon_{ki}(\boldsymbol{x},\boldsymbol{y})}{\partial x_n}\left(\delta_{kp}+\frac{\partial R^{(p)}}{\partial y_k}\right)\frac{\partial\psi^{(rs)}}{\partial y_i}$$
$$+e_{kij}(\boldsymbol{x},\boldsymbol{y})\left(\delta_{kp}+\frac{\partial R^{(p)}}{\partial y_k}\right)\frac{\partial^2\chi_i^{(rs)}}{\partial y_j\partial x_n}$$
$$-\epsilon_{ki}(\boldsymbol{x},\boldsymbol{y})\left(\delta_{kp}+\frac{\partial R^{(p)}}{\partial y_k}\right)\frac{\partial^2\psi^{(rs)}}{\partial y_i\partial x_n}\Bigg]\mathrm{d}Y\Bigg\} \quad (28)$$

- Sensitivity of Dielectric Properties

Deriving Eq. (25) in relation to design variable x_n and considering Eqs. (21) and (22), we get after some algebra manipulation:

$$\frac{\partial\epsilon_{pq}^h(\boldsymbol{x})}{\partial x_n}=$$
$$\frac{1}{|Y|}\Bigg\{\int_Y\Bigg[\frac{\partial\epsilon_{ij}(\boldsymbol{x},\boldsymbol{y})}{\partial x_n}\left(\delta_{ip}+\frac{\partial R^{(p)}}{\partial y_i}\right)\left(\delta_{jq}+\frac{\partial R^{(q)}}{\partial y_j}\right)$$
$$-\frac{\partial e_{kij}(\boldsymbol{x},\boldsymbol{y})}{\partial x_n}\left(\delta_{kp}+\frac{\partial R^{(p)}}{\partial y_k}\right)\frac{\partial\Phi_i^{(q)}}{\partial y_j}$$
$$+\epsilon_{ij}(\boldsymbol{x},\boldsymbol{y})\left(\delta_{ip}+\frac{\partial R^{(p)}}{\partial y_i}\right)\frac{\partial^2 R^{(q)}}{\partial y_j\partial x_n}$$
$$-e_{kij}(\boldsymbol{x},\boldsymbol{y})\left(\delta_{kp}+\frac{\partial R^{(p)}}{\partial y_k}\right)\frac{\partial^2\Phi_i^{(q)}}{\partial y_j\partial x_n}\Bigg]\mathrm{d}Y\Bigg\} \quad (29)$$

Expressions (27), (28), and (29) cannot be further simplified. Terms $\frac{\partial^2\Phi_k^{(m)}}{\partial y_l\partial x_n}$, $\frac{\partial^2 R^{(m)}}{\partial y_k\partial x_n}$, $\frac{\partial^2\chi_i^{(mn)}}{\partial y_j\partial x_n}$, and $\frac{\partial^2\psi^{(mn)}}{\partial y_i\partial x_n}$ can be obtained by deriving Eqs. (19), (20), (21), and (22) in relation to design variable x_n resulting in:

$$\int_Y\left[c_{ijkl}(\boldsymbol{x},\boldsymbol{y})\frac{\partial^2\chi_i^{(mn)}}{\partial y_i\partial x_n}+e_{ikl}(\boldsymbol{x},\boldsymbol{y})\frac{\partial^2\psi^{(mn)}}{\partial y_i\partial x_n}\right]\varepsilon_{kl}(\mathbf{v})\mathrm{d}Y$$
$$=-\int_Y\Bigg[\frac{\partial c_{ijkl}(\boldsymbol{x},\boldsymbol{y})}{\partial x_n}\left(\delta_{im}\delta_{jn}+\frac{\partial\chi_i^{(mn)}}{\partial y_j}\right)$$
$$+\frac{\partial e_{ikl}(\boldsymbol{x},\boldsymbol{y})}{\partial x_n}\frac{\partial\psi^{(mn)}}{\partial y_i}\Bigg]\varepsilon_{kl}(\mathbf{v})\mathrm{d}Y,\ \ \forall\ \mathbf{v}\in H_{per}(Y,R^3)$$

$$\int_Y\left[e_{kij}(\boldsymbol{x},\boldsymbol{y})\frac{\partial^2\chi_i^{(mn)}}{\partial y_j\partial x_n}-\epsilon_{ik}(\boldsymbol{x},\boldsymbol{y})\frac{\partial^2\psi^{(mn)}}{\partial y_i\partial x_n}\right]\frac{\partial w}{\partial y_k}\mathrm{d}Y$$
$$=-\int_Y\Bigg[\frac{\partial e_{kij}(\boldsymbol{x},\boldsymbol{y})}{\partial x_n}\left(\delta_{im}\delta_{jn}+\frac{\partial\chi_i^{(mn)}}{\partial y_j}\right)$$
$$-\frac{\partial\epsilon_{ik}(\boldsymbol{x},\boldsymbol{y})}{\partial x_n}\frac{\partial\psi^{(mn)}}{\partial y_i}\Bigg]\frac{\partial w}{\partial y_k}\mathrm{d}Y\ ,$$
$$\forall w\in H_{per}(Y)$$

$$\int_Y\left[c_{klij}(\boldsymbol{x},\boldsymbol{y})\frac{\partial^2\Phi_k^{(m)}}{\partial y_l\partial x_n}+e_{kij}(\boldsymbol{x},\boldsymbol{y})\frac{\partial^2 R^{(m)}}{\partial y_k\partial x_n}\right]\varepsilon_{ij}(\mathbf{v})\mathrm{d}Y$$
$$=-\int_Y\left[\frac{\partial c_{klij}(\boldsymbol{x},\boldsymbol{y})}{\partial x_n}\frac{\partial\Phi_k^{(m)}}{\partial y_l}+\frac{\partial e_{kij}(\boldsymbol{x},\boldsymbol{y})}{\partial x_n}\left(\delta_{mk}+\frac{\partial R^{(m)}}{\partial y_k}\right)\right]$$
$$\times\varepsilon_{ij}(\mathbf{v})\mathrm{d}Y,\ \ \forall\mathrm{v}\in H_{per}(Y,R^3)$$

$$\int_Y\left[e_{kij}(\boldsymbol{x},\boldsymbol{y})\frac{\partial^2\Phi_i^{(m)}}{\partial y_j\partial x_n}-\epsilon_{ik}(\boldsymbol{x},\boldsymbol{y})\frac{\partial^2 R^{(m)}}{\partial y_i\partial x_n}\right]\frac{\partial w}{\partial y_k}\mathrm{d}Y$$
$$=-\int_Y\left[\frac{\partial e_{kij}(\boldsymbol{x},\boldsymbol{y})}{\partial x_n}\frac{\partial\Phi_i^{(m)}}{\partial y_i}-\frac{\partial\epsilon_{ik}(\boldsymbol{x},\boldsymbol{y})}{\partial x_n}\left(\delta_{mi}+\frac{\partial R^{(m)}}{\partial y_i}\right)\right]$$
$$\frac{\partial w}{\partial y_k}\mathrm{d}Y,\forall w\in H_{per}(Y)$$

The system of equations above is solved by using the finite element method.

B.2
Sensitivity of objective functions

The sensitivity of objective functions (performance characteristics) can be obtained by deriving Eqs. (11) in relation to design variables x_n and expressing the result as a function of the sensitivities of the material coefficients presented above. The derivation of Eqs. (11) is straightforward, so it will not be presented here.

References

1. **ANSI/IEEE Std 176-1978** (1984): IEEE Standard on Piezoelectricity. Special Issue of Trans. on Sonics and Ultrasonics SU-31, 2
2. **Avellaneda, M.; Swart, P. J.** (1994): The role of matrix porosity and Poisson's ratio in the design of high-sensitivity piezocomposite transducers. Adaptive Structures and Composite Materials: Analysis and Application – ASME, Aerospace Division, AD 45, 59–66
3. **Fonseca, J. S. O.; Kikuchi, N.** (1995): Optimal Design of Microstructures. Proc. Third U.S. National Congress on Computational Mechanics, Dallas, Texas, 77
4. **Fonseca, J. S. O.; Kikuchi, N.** (1996): Design of Microstructures of Periodic Composite Materials (to be published)
5. **Galka, A.; Telega, J. J.; Wojnar, R.** (1992): Homogenization and Thermopiezoelectricity. Mechanics Research Communications 19, 4, 315–324
6. **Gibiansky, L. V.; Torquato, S.** (1995): On the Use of Homogenization Theory to Optimally Design Piezocomposites for Hydrofone Applications (to be published)
7. **Hanson, R.; Hiebert, K.** (1981): A Sparse Linear Programming Subprogram. Sandia National Laboratories. Technical Report SAND81-0297

8. **Hashin, Z.; Shtrikman, S. (1963):** A Variational Approach of the Theory of Elastic Behavior of Multiphase materials. Journal of the Mechanics and Physics of Solids, 11, 127–140
9. **Hayward, G.; Bennett, J.** (1996): Assessing the Influence of Pillar Aspect Ratio on the Behavior of 1-3 Connectivity Composite Transducers. IEEE Trans. on Ultrasonics, Ferroelectrics, and Frequency control 43, 1, 98–108
10. **Hossack, J. A.; Hayward, G.** (1991): Finite Element Analysis of 1-3 Composite Transducers. IEEE Trans. on Ultrasonics, Ferroelectrics, and Frequency Control 38, 6, 618–629
11. **Naillon, M.; Coursant, R. H.; Besnier, F.** (1983): Analysis of Piezoelectric Structures by a Finite Element Method. Acta Electronica, 25, 4, 341–362
12. **Ristic, V. M.** (1983): Principles of Acoustic Devices. New York: John Wiley & Sons
13. **Sanchez-Hubert, J.; Sanchez-Palencia, E.** (1992): Introduction aux Méthodes Asymptotiques et à l' Homogénéisation. Paris: Masson
14. **Sigmund, O.** (1995): Tailoring Materials with Prescribed Elastic Properties. Mechanics of Materials 20, 351–368
15. **Sigmund, O.; Torquato, S.** (1996): Design of Materials with Extreme Thermal Expansion Using a Three-Phase Topology Optimization Method. Danish Center for Applied Mathematics and Mechanics, Report No. 525
16. **Smith, W. A.** (1984): Optimizing Electromechanical Coupling in Piezocomposites Using Polymers with Negative Poisson's Ratio. IEEE 1991 Ultrasonics Symposium Proc. (Cat. No. 91CH3079-1), Orlando, Florida, 1, 661–666
17. **Smith, W. A.; Auld, B. A.** (1991): Modeling 1-3 Composite Piezoelectrics: Thickness-Mode Oscillations. IEEE Trans. on Ultrasonics, Ferroelectrics, and Frequency Control 38, 1, 40–47
18. **Smith, W. A.** (1992): Limits to the Enhancement of Piezoelectric Transducers Achievable by Materials Engineering. IEEE 1992 Ultrasonics Symposium Proc. (Cat. No. 92CH3118-7), Tucson, Arizona, 1, 697–702
19. **Smith, W. A.** (1993): Modeling 1-3 Composite Piezoelectrics: Hydrostatic Response. IEEE Trans. on Ultrasonics, Ferroelectrics, and Frequency Control 40, 1, 41–49
20. **Telega, J. J.** (1990): Piezoelectricity and Homogenization. Application to Biomechanics. Continuum Models and Discrete Systems 2, 220–230. London: G.A. Maugin, Longman
21. **Tiersten, H. F.** (1967): Hamilton's Principle for Linear Piezoelectric Media. IEEE 1967 Proc., 1523–1524